

TO: J. MENARD, C. NEUMEYER

FROM: S.P. GERHARDT (PPPL), M.L. REINKE (ORNL)

SUBJECT: HEAT FLUXES ON THE CENTERSTACK ANGLED SURFACE AND FAR OUTBOARD DIVERTOR REGIONS (ROWS 3-4)

1: Objective	1
2: Results	1
3: Methods	3
4: L-mode Equilibrium Scans That Place Heat Fluxes on the OBD Row 4 and CSAS	4
4.1 DN Cases	4
4.2: LSN L-Mode Cases	10
4.3: USN L-mode	13
5: H-Mode Sweeps on IBDV Placing Power on the CSAS	13
6: H-Mode Scans on Row 4 Motivated by Materials and PFC TSG	16
7: Lower Triangularity Scans That Place Power on Row 3 Tiles ($0.85 < R < 0.92$)	18
References	20

1: Objective

This memo describes studies of heat fluxes on the Center Stack Angled Surface (CSAS) ($1.27 < |Z| \text{ [m]} < 1.05$) and far regions of the Outboard Divertor (OBD) ($R \text{ [m]} > \sim 0.85$). These regions are generally only loaded with plasma heat for specific equilibria, which are described here. Recommended heat flux requirements are provided in Section 2 with subsequent sections describing the modeling and analysis that led to these recommendations. Companion documents for PFCR-MEMO-009 [1] and -010 [2] will describe similar results for the Inboard Divertor Vertical (IBDV) and Inboard Divertor Horizontal (IBDH) & near OBD ($0.6 < R \text{ [m]} < 0.85$), respectively.

The basis for these studies are the so-called Topical Science Group (TSG) memos [3-8], written by the TSG leaders and describing their view of plasma facing component (PFC) requirements and scenarios that drive those requirements.

2: Results

Tables 2.1, 2.2 and 2.3 are based on TSG-inspired modeling, described in sections below. For each PFC region, multiple cases are specified which should span the limiting cases of heat flux, duration and angles of incidence. Rather than give single values, designs should be first qualified against each of these independently. For example, the use of poloidal flux expansion makes surface heat flux related to the angle of incidence, so is

excessive to qualify a design at the highest heat flux and the shallowest angle of incidence. A first attempt should apply heat flux uniformly over these surfaces as generally this represents time-averaged heat fluxes from sweeping. More detailed data for modeling is available upon request to the authors.

For the CSAS, recommended design values follow from L-mode cases discussed in Section 4.2. These requirements are based on L-mode equilibria using a range of I_p and B_T with the largest power applied for each case. Note durations are all ~ 2.0 seconds.

CSAS	Case # ->	1	2	3
Max Angle	degrees	9.2	4.0	12
Min Angle	degrees	7.3	2.5	9.5
Heat Flux	MW/m ²	5.2	1.0	3.6
Duration	sec	2.0	2.0	2.0
Reference Scenario		High I_p/B_T LSN L-Mode, 3 MW	Low I_p/B_T LSN L-Mode, 1.5 MW	High I_p/B_T LSN L-Mode, 2 MW

Table 2.1: Suggested heat flux requirements for the Center Stack Angle Section.

Requirements for the far region of the OBD are in Tables 2.2 and 2.3, where this is a significant enough difference as to warrant further separation. OBD-R3 will be used in high power H-mode scenarios, while OBD-R4/R5 will generally be used in lower power L-mode discharges and also must account for the non-axisymmetry of the PFCs due to diagnostic cutouts.

OBD-R3	Case # ->	1	2
Max Angle	degrees	7.9	10
Min Angle	degrees	2.2	8.5
Heat Flux	MW/m ²	10.5	3.0
Duration	sec	1.0	5.0
Reference Scenario		short duration high power (DivSol 8- 07)	MPFC Far-OBD MAPP Scan

Table 2.2: Suggested heat flux requirements for OBD-R3 ($0.85 < R < 0.92$).

<u>OBD-R4/5</u>	Case # ->	1	2	3	4
Max Angle	degrees	14	8.2	16.5	10
Min Angle	degrees	9.2	4.8	13.5	8.5
Heat Flux	MW/m ²	4.3	1.8	3.0	3.0
Duration	sec	2.0	2.0	2.0	5.0
Reference Scenario		High I _p /B _T LSN Swept L- Mode	Low I _p /B _T LSN Swept L- Mode	High I _p /B _T LSN Swept L- Mode	MPFC Far- OBD MAPP Scan

Table 2.3: Suggested heat flux requirements for OBD-R4 and OBD-R5 ($R > 0.92$).

3: Methods

Various equilibrium scans were done via the ISOLVER equilibrium code. This code, written by Jon Menard, is a free boundary equilibrium code with various options for controlling the boundary shape and coil currents. In particular, any coil current can be hard coded, or used in the shape controller. Some new versions of the code additionally have strike-point control capability, though this was not used in the present studies.

The equilibrium is highly dependent on the plasma profiles. As run here, the pressure and current profiles from NSTX or NSTX-U equilibria were used. Both L-mode and H-mode profiles were selected.

Once selected scans were created, they were entered into IDL-based codes to compute heat flux to axisymmetric PFC surfaces as outlined in PFCR-MEMO-004 (eventually will be superseded by PFCR-MEMO-007). A given input power and radiated power fraction defines the total exhaust power with defined rules, based on the equilibrium, setting the fraction of power to each divertor surface. The outboard midplane parallel heat flux, $q_{||}$, profile is defined using the standard exponential (λ_q) convolved with a spreading factor (S) as described in [T. Eich, *et al.* PRL **107**, 215001 (2011)]. Various scalings can be used to extrapolate (S, λ_q) into new NSTX-U operational space. The equilibrium is used to map $q_{||}$ to boundary surfaces and define the local angle of incidence, α , which defines the perpendicular heat flux, q_{perp} , to the surface. Calculations are based on the original NSTX-U PFC boundary. If that boundary is moved as in the expected CDR designs, the heat fluxes for the chosen equilibria may change.

For the H-mode heat flux modeling, Heuristic Drift Scaling using equations (7), (9) and (10) in [T. Eich, *et al.* PRL **107**, 215001 (2011)] for the heat flux width, λ_q , was assumed, while for L-mode plasmas this was doubled, representing the common

empirical result that the L-mode heat flux with is approximately twice that of an H-mode. Scaling from Figure 6 in [M. Makowski, *et al.* Physics of Plasmas **19**, 056122 (2012)] was used for the heat flux spreading factor, \square . Radiated power is fixed at 30% for both L-mode and H-mode. Power splitting for the divertors are summarized in Table 3.1. A hyperbolic tangent function is used to estimate the sharing for values in the range of $0 < |dr_{sep}/\lambda_q| < 5$.

EQ. CASE	Inner	Outer
LSN	30%	70%
DN	20%	80%
USN	45%	55%

Table 3.1: Power sharing between inner and outer divertors used in the analysis.

Strike point sweeping is approximated by providing a series of static equilibria and interpolating the heat flux profile in between to generate a smooth, time-evolving heat flux profile, from which the average heat flux is computed at each (R,Z) via $q_{AVE} = \frac{1}{\Delta t} \int_0^{\Delta t} q_{perp} dt$, which is independent of the sweep frequency.

Sections 4-7 describe how these methods are applied to estimate the heat flux requirements for the CSAS, and the R3-R5 regions of the OBD. Section 4 includes more detail on the step-by-step process, while Sections 5-7 highlight the input and output data, and give a brief description of the motivation.

4: L-mode Equilibrium Scans That Place Heat Fluxes on the OBD Row 4 and CSAS

Scans of L-mode equilibria were generated, based on requests from the Transport and Turbulence TSG [1]. These are limited to a duration of 2 seconds, based on the observed flux consumption of L-mode plasmas in NSTX-U.

Given that these cases represent L-mode plasmas, an input power of 3 MW is assumed. This is conservative for a LSN L-mode, in that the plasma would likely transition to H-mode or reach an MHD stability limit. However, it must be noted that and USN equilibrium with similar shape, which approximately doubles the L-H threshold, is of interest for PED, T&T and EP experiments.

4.1 DN Cases

These L-mode scans were done for $[I_p, B_T, P_{inj}]$ triplets of [800 kA, 0.75 T, 2 MW], [1000 kA, 1.0 T, 3 MW] and [500 kA, 1.0 T, 1.5 MW]. The individual file names for the GEQDSKs and additional information are provided in Tables 4.1.1, 4.1.2, and 4.1.3.

Files are organized by TSG and currently located at: /p/nstxusr/nstx-users/sgerhard/PFCs/NSTXU_Recovery_Requirements/TSG_geqds

In Table 4.1.1, the GEQDSK files have two numbers at the end of each name. The first is the ratio of the PF-1a current to the plasma current, while the second is the ratio of the PF-2 current to the plasma current. The currents are up-down symmetric. The currents used in the table use the full available amplitude headroom, and are the limiting factor in the scans.

DN Scans, $i_i=1.4$, $I_p=800$ kA					
I_p (kA)	800	i_i	1.4	P_{inj} (MW)	2
B_T (T)	0.75	dr_{sep} (cm)	0	Underlying Equilibrium	204062, EFIT01, 1.25 seconds
1-05b			1-05c		
g204062.01250_TT_1-05_0.024_0.010			g204062.01250_TT_1-05_0.024_0.006		
g204062.01250_TT_1-05_0.022_0.012			g204062.01250_TT_1-05_0.022_0.008		
g204062.01250_TT_1-05_0.020_0.014			g204062.01250_TT_1-05_0.020_0.010		
g204062.01250_TT_1-05_0.018_0.016			g204062.01250_TT_1-05_0.018_0.012		
g204062.01250_TT_1-05_0.016_0.018			g204062.01250_TT_1-05_0.016_0.014		
g204062.01250_TT_1-05_0.014_0.020			g204062.01250_TT_1-05_0.014_0.016		
g204062.01250_TT_1-05_0.012_0.022			g204062.01250_TT_1-05_0.012_0.018		

Table 4.1.1: Equilibrium files for two double null L-mode scans at $I_p=800$ kA and $B_T=0.75$ T.

DN Scans, $i_i=1.4$, $I_p=1000$ kA					
I_p (kA)	1000	i_i	1.4	P_{inj} (MW)	3
B_T (T)	1	dr_{sep} (cm)	0	Underlying Equilibrium	204062, EFIT01, 1.25 seconds
1-06a			1-06b		
g204062.01250_TT_1-06_0.008_0.016			g204062.01250_TT_1-06_0.012_0.016		
g204062.01250_TT_1-06_0.010_0.014			g204062.01250_TT_1-06_0.014_0.014		
g204062.01250_TT_1-06_0.012_0.012			g204062.01250_TT_1-06_0.016_0.012		
g204062.01250_TT_1-06_0.014_0.010			g204062.01250_TT_1-06_0.018_0.010		

Table 4.1.2: Equilibrium files for two double null L-mode scans at $I_p=1000$ kA and $B_T=1.0$ T.

DN Scans, $I_i=1.4$, $I_p=500$ kA					
I_p (kA)	500	I_i	1.4	P_{inj} (MW)	3
B_T (T)	1	dr_{sep} (cm)	0	Underlying Equilibrium	204062, EFIT01, 1.25 seconds
1-07a			1-07b		
g204062.01250_TT_1-07_0.010_0.016			g204062.01250_TT_1-07_0.008_0.014		
g204062.01250_TT_1-07_0.012_0.014			g204062.01250_TT_1-07_0.010_0.012		
g204062.01250_TT_1-07_0.014_0.012			g204062.01250_TT_1-07_0.012_0.010		
g204062.01250_TT_1-07_0.016_0.010			g204062.01250_TT_1-07_0.014_0.008		
g204062.01250_TT_1-07_0.018_0.008			g204062.01250_TT_1-07_0.016_0.006		

Table 4.1.3: Equilibrium files for two double null L-mode scans at $I_p=500$ kA and $B_T=1.0$ T.

Typical equilibrium a shapes for the Scans 1-05b and 1-05c are shown in Figure 4.1.1. These incorporate scans of the outer strike-point radius and inner strike-point height.

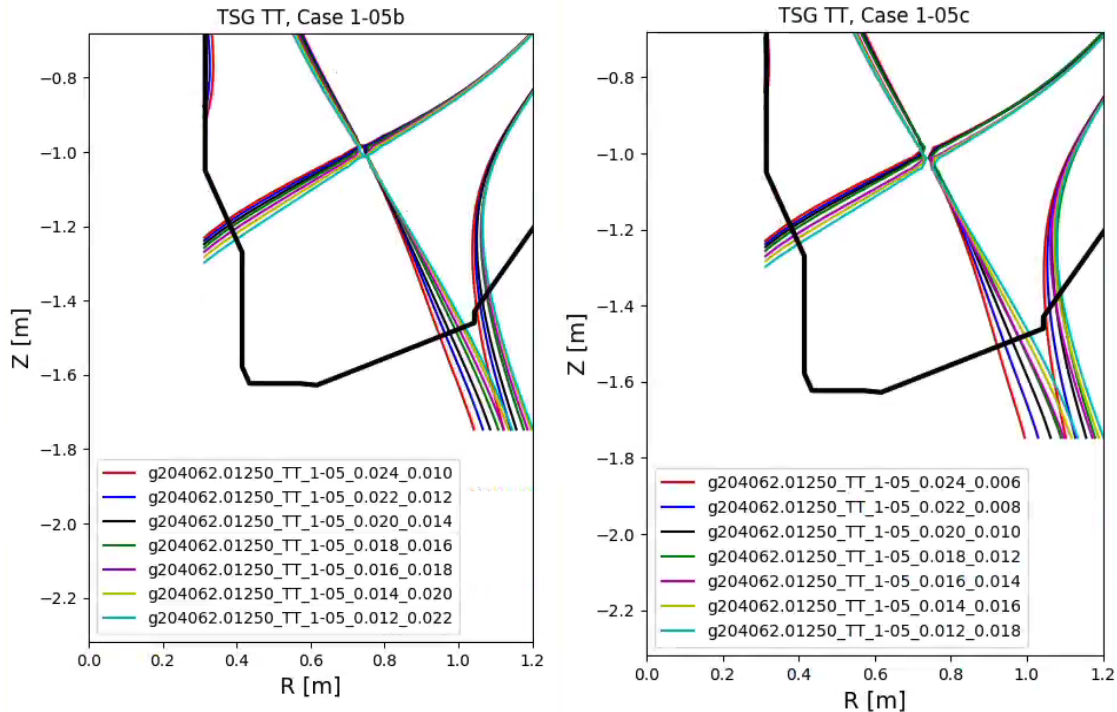


Fig. 4.1.1: L-mode DN equilibria from Scans 1-05b and 1-05c.

Typical heat flux profiles for Scan 1-05b are shown in Fig. 4.1.2 (lower outer strike-point) and 4.3 (lower inner strike-point).

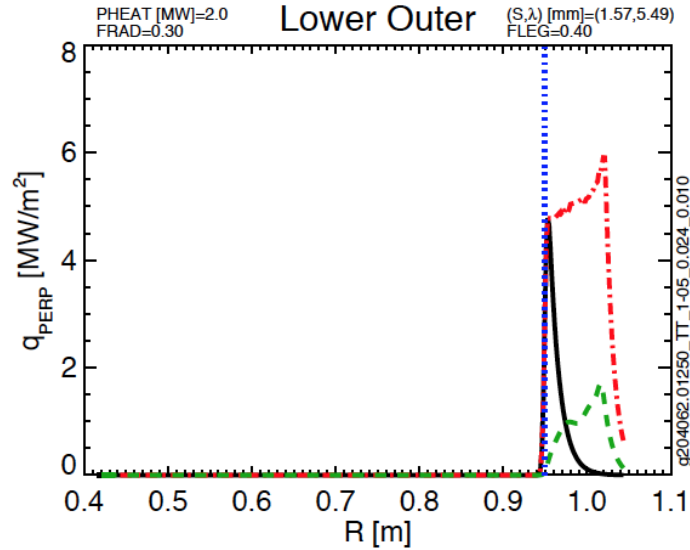


Fig. 4.1.2: Lower outer strikepoint heat flux, as a function of major radius, for Scan 1-05b.

Considering Figure 4.1.2, the heat flux profile is plotted as a function of major radius. The vertical dash-dot blue line represents the location of the strike point on the divertor, for the time (equilibrium) under consideration. There are three curves, showing:

- **green dashed:** averaged heat flux over the sweep
- **red dot-dashed:** peak heat flux encountered at each location during the sweep
- **black solid:** heat flux profile for the single equilibrium

From the plot, it can be seen that typical stationary powers at the outer strikepoint from this case are 5-6 MW/m², but reduce to < 2 MW/m² when sweeping is applied. From Figure 4.1.3, typical powers at the inner strikepoint are 2.5 MW/m², reduced to ~1 MW/m² when sweeping is applied.

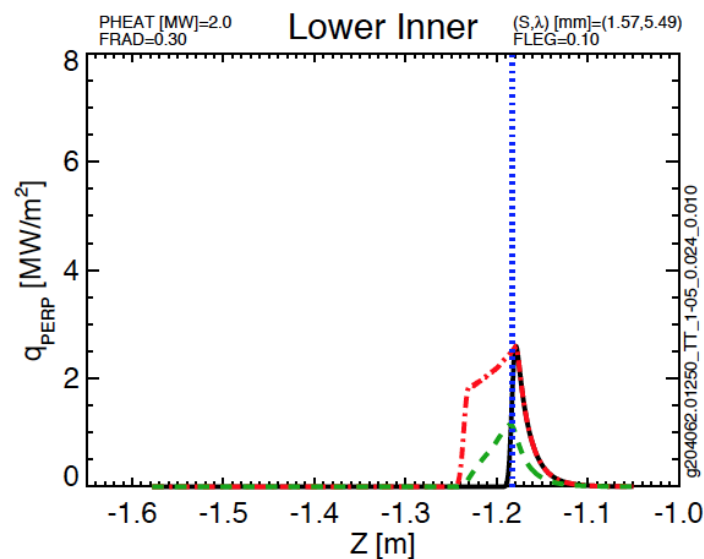


Fig. 4.1.3: Inner strikepoint heat flux as a function of vertical height, for scan 1-05b.

There are field line angles with these scans, as shown in Figs. 4.1.4 and 4.1.5. Considering Fig. 4.1.4, the total angle is plotted as a function of major radius. The vertical dash-dot blue line represents the location of the strike point on the divertor, for the time (equilibrium) under consideration. There are three curves, showing:

- **green dashed:** averaged field line angle over the sweep
- **red dot-dashed:** maximum and minimum field line angles at any point during the sweep
- **black solid:** single profile for the equilibrium under consideration

From Fig. 4.4, it can be seen that typical angles on the outer target in the region of high heat flux, $0.95 < R < 1.05$ (see Fig. 4.2) are 13 to 18 degrees. From Fig. 4.5, typical angle ranges on the vertical target are 4 to 14 degrees.

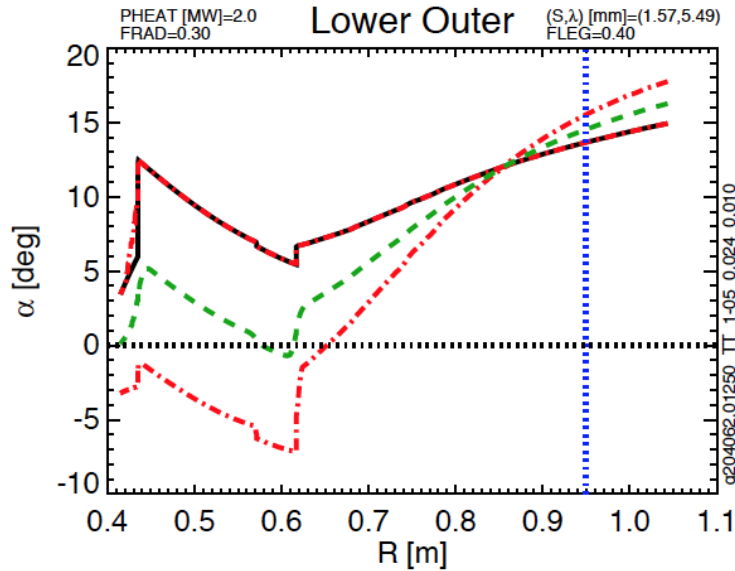


Fig. 4.1.4: Outer strikepoint angles as a function of major radius, for scan 1-05b.

These calculations have been made for the double-null equilibria in Tables 4.1.1 to 4.1.3, and the results are summarized in Tables 4.1.4 and 4.1.5. Bold, red text is used to highlight the extreme values of interest. Not surprisingly, these values are less than those shown in Section 4.2 for LSN cases and are not driving the requirements listed in Tables 2.1 and 2.3.

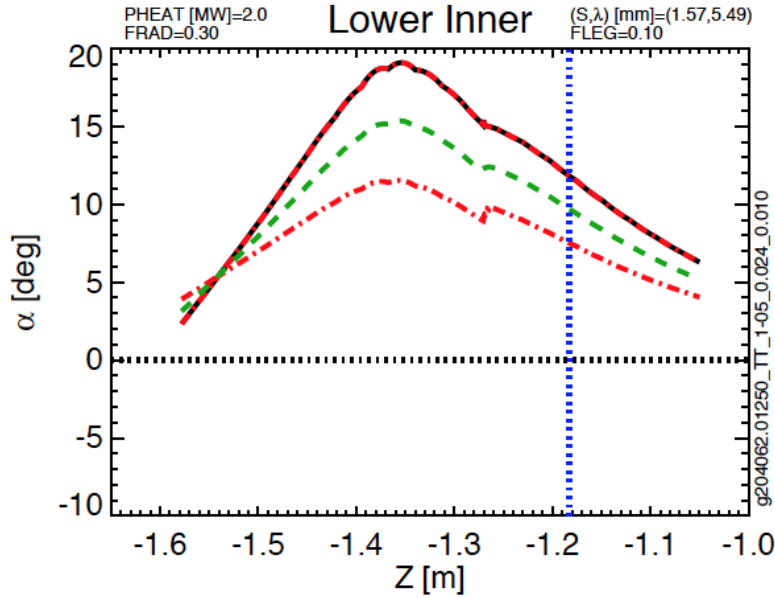


Fig. 4.1.5: Inner strikepoint angles as a function of vertical height, for scan 1-05b.

Scan	[I_p, B_T, P_{inj}]	Radial Range of OSP Sweep	Peak Instantaneous Heat Flux	Peak Swept Heat Flux	Angle Range at R_{min}	Angle Range at R_{max}
---	kA, T, MW	m	MW/m ²	MW/m ²	deg.	deg.
1-05b	[800, 0.75, 2]	[0.95, 1.02]	5.9	1.7	13.7	17.3
1-05c	[800, 0.75, 2]	[0.92, 1.01]	4.9	1.3	11.2	14.7
1-06a	[1000, 1, 3]	[0.97, 1.02]	8.0	2.9	9.6	11.5
1-06b	[1000, 1, 3]	[0.96, 1.00]	7.5	3.5	11.0	12.8
1-07a	[500, 1, 3]	[0.94, 1.01]	2.2	1.0	5.0	6.2
1-07b	[500, 1, 3]	[0.92, 1.01]	2.1	0.93	4.0	5.2

Table 4.1.5: OBD parameters for DN L-mode Scans from T&T

Scan	[I_p, B_T, P_{inj}]	Vertical Range of ISP Sweep	Peak Instantaneous Heat Flux	Peak Swept Heat Flux	Angle Range at Z_{min}	Angle Range at Z_{max}
---	kA, T, MW	m	MW/m ²	MW/m ²	deg.	deg.
1-05b	[800, 0.75, 2]	[1.18, 1.24]	2.6	1.2	11.8	9.1
1-05c	[800, 0.75, 2]	[1.18, 1.24]	2.5	1.1	11.5	8.7
1-06a	[1000, 1, 3]	[1.22, 1.27]	3.2	1.5	8.0	6.0
1-06b	[1000, 1, 3]	[1.20, 1.23]	3.8	2.1	9.2	7.9
1-07a	[500, 1, 3]	[1.20, 1.24]	0.8	0.6	4.4	3.5

1-07b	[500,1,3]	[1.21,1.26]	0.8	0.5	4.1	3.0
-------	-----------	-------------	-----	-----	-----	------------

Table 4.1.6: CSAS parameters for DN L-mode Scans from T&T

4.2: LSN L-Mode Cases

Lower single null L-mode cases have been constructed in a manner very similar to the double-null cases. These cases also have $[I_p, B_T, P_{inj}]$ triplets of [800 kA, 0.75 T, 2 MW], [1000 kA, 1.0 T, 3 MW] and [500 kA, 1.0 T, 1.5 MW]. However, being LSN, they deposit all power on the lower targets, with no upper target power.

LSN Scans, $I_i=1.4$, $I_p=800$ kA					
I_p (kA)	800	I_i	1.4	P_{inj} (MW)	2.0
B_T (T)	0.75	dr_{sep} (cm)	-1.5	Underlying Equilibrium	204062, EFIT01, 1.25 seconds
2-04a			2-04c		
g204062.01250_TT_2-04_0.024_0.010			g204062.01250_TT_2-04_0.024_0.006		
g204062.01250_TT_2-04_0.022_0.012			g204062.01250_TT_2-04_0.022_0.008		
g204062.01250_TT_2-04_0.020_0.014			g204062.01250_TT_2-04_0.020_0.010		
g204062.01250_TT_2-04_0.018_0.016			g204062.01250_TT_2-04_0.018_0.012		
g204062.01250_TT_2-04_0.016_0.018			g204062.01250_TT_2-04_0.016_0.014		
g204062.01250_TT_2-04_0.014_0.020			g204062.01250_TT_2-04_0.014_0.016		

Table 4.2.1: L-mode scans for $I_p=0.8$ MA, $B_T=0.75$ T, in a LSN configuration

In Tables 4.2.1, 4.2.2, and 4.2.3, the file names have two numbers at the end of each name. The first is the ratio of the PF-1aL current to the plasma current, while the second is the ratio of the PF-2L current to the plasma current. The PF-2U coil current was set to zero, while the PF-1aU current was adjusted to achieve the desired dr_{sep} values. Again, the currents used in the table use the full available headroom, and are the limiting factor in the scans.

In each scan, both the OSP and ISP are scanned. There are significant limitations on the range of the scans, due to the inability of the PF set to easily shape the plasma at these high values of internal inductance. The resulting parameters of the scans are as follows from Tables 4.2.4 and 4.2.5.

LSN Scans, $I_i=1.4$, $I_p=1000$ kA					
I_p (kA)	1000	I_i	1.4	P_{inj} (MW)	3
B_T (T)	1	dr_{sep} (cm)	-1.5	Underlying Equilibrium	204062, EFIT01, 1.25 seconds
2-05a			2-05b		
g204062.01250_TT_2-05_0.006_0.018			g204062.01250_TT_2-05_0.010_0.018		
g204062.01250_TT_2-05_0.008_0.016			g204062.01250_TT_2-05_0.012_0.016		
g204062.01250_TT_2-05_0.010_0.014			g204062.01250_TT_2-05_0.014_0.014		
g204062.01250_TT_2-05_0.012_0.012			g204062.01250_TT_2-05_0.016_0.012		
g204062.01250_TT_2-05_0.014_0.010			g204062.01250_TT_2-05_0.018_0.010		
g204062.01250_TT_2-05_0.016_0.008					

Table 4.2.2: L-mode scans for $I_p=1$ MA, $B_T=1$ T, in a LSN configuration

LSN Scans, $I_i=1.4$, $I_p=500$ kA					
I_p (kA)	500	I_i	1.4	P_{inj} (MW)	1.5
B_T (T)	1	dr_{sep} (cm)	-1.5	Underlying Equilibrium	204062, EFIT01, 1.25 seconds
2-06b			2-06c		
g204062.01250_TT_2-06_0.006_0.018			g204062.01250_TT_2-06_0.010_0.022		
g204062.01250_TT_2-06_0.008_0.016			g204062.01250_TT_2-06_0.012_0.020		
g204062.01250_TT_2-06_0.010_0.014			g204062.01250_TT_2-06_0.014_0.018		
g204062.01250_TT_2-06_0.012_0.012			g204062.01250_TT_2-06_0.016_0.016		
g204062.01250_TT_2-06_0.014_0.010			g204062.01250_TT_2-06_0.018_0.014		
g204062.01250_TT_2-06_0.016_0.008			g204062.01250_TT_2-06_0.020_0.012		

Table 4.2.3: L-mode scans for $I_p=0.5$ MA, $B_T=1$ T, in a LSN configuration

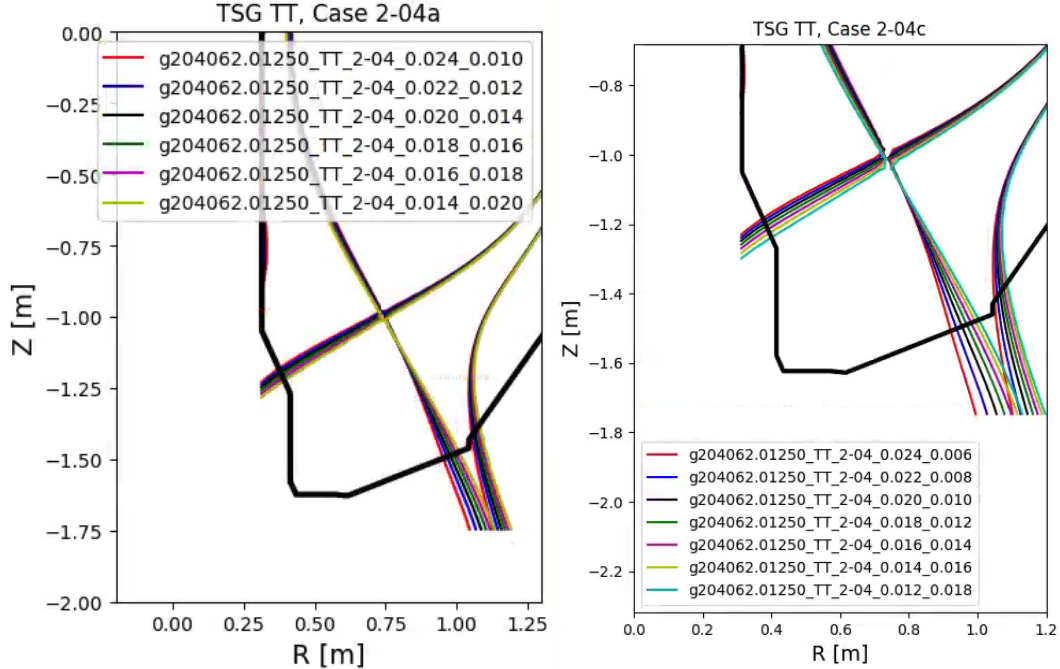


Figure 4.2.4: L-mode lower single null equilibria from scans 2-04.

Scan	$[I_p, B_T, P_{inj}]$	Radial Range of OSP Sweep	Peak Instantaneous Heat Flux	Peak Swept Heat Flux	Angle Range at R_{min}	Angle Range at R_{max}
---	kA,T,MW	m	MW/m ²	MW/m ²	degrees	degrees
2-04a	[800,0.75,2]	[0.95,1.01]	9.4	2.7	13.6	16.6
2-04c	[800,0.75,2]	[0.92, 1.00]	8.2	2.1	11.2	14.7
2-05a	[1000,1,3]	[0.93,1.01]	13.3	3.3	9.3	12.4
2-05b	[1000,1,3]	[0.94,1.00]	14.7	4.3	11.2	13.6
2-06b	[500,1,1.5]	[0.93,1.01]	2.4	1.0	4.8	6.4
2-06c	[500,1,1.5]	[0.96,1.01]	4.4	1.8	6.7	8.2

Table 4.2.4: Row 4 OBD parameters for LSN L-mode Scans

The results in Table 4.2.4 are used to inform the Case#1-Case#3 requirements in Table 2.3 for the OBD R4/5. Operation for short pulse, at high power is included as Case#1, while others influence the range of expected field line angles to help inform any decisions related to optimizing tile shaping (e.g. around fastener access holes). The highest field line angle case, even at more modest heating, will be important for this region to scope the impact of the large diagnostic cutouts.

Scan	$[I_p, B_T, P_{inj}]$	Vertical Range of ISP Sweep	Peak Instantaneous Heat Flux	Peak Swept Heat Flux	Angle Range at Z_{min}	Angle Range at Z_{max}
---	kA,T,MW	m	MW/m ²	MW/m ²	degrees	degrees
2-04a	[800,0.75,2]	[1.18,1.22]	7.4	3.6	11.8	9.6
2-04c	[800,0.75,2]	[1.18,1.24]	7.2	3.1	11.5	8.7
2-05a	[1000,1,3]	[1.21,1.30]	9.7	3.5	8.4	5.1
2-05b	[1000,1,3]	[1.20,1.25]	10.8	5.2	9.2	7.3
2-06b	[500,1,1.5]	[1.20,1.29]	1.4	0.8	4.1	2.5
2-06c	[500,1,1.5]	[1.19,1.24]	2.4	1.5	4.9	3.8

Table 4.2.5: CSAS parameters for LSN L-mode Scans

The results in Table 4.2.5 are used to inform the Case#1-Case#3 requirements in Table 2.1 for the CSAS. Operation for short pulse, at high power is included as Case#1, while others influence the range of expected field line angles to help inform any decisions related to optimizing tile shaping. These requirements, along with those taken from Table 4.2.4 should include a large fraction of the L-mode operations scope in LSN and DN requested by the T&T and EP TSGs.

4.3: USN L-mode

The equilibria generated in Section 4.2 can be generated for USN cases and new tables created, but it's simpler just to use Tables 4.2.4 and 4.2.5 and re-calculate the peak powers expected. The OBD power will drop, but the power and the CSAS will increase by 50%. Thus instead of 10.8 MW/m² and 5.2 MW/m² being the maximum peak and average expected for the CSAS, as per case 2-05b, the upper CSAS may see up to 16.2 MW/m² and 7.8 MW/m², respectively. This is beyond the expected allowables for this region without significant engineering investment, so it is recommended to use Table 4.2.6 as the CSAS requirements, with the caveat that USN L-mode cases need to be qualified for a input power and pulse length based on the completed design.

5: H-Mode Sweeps on IBDV Placing Power on the CSAS

It is likely that some inner strike-point sweeps on the IBDV will place power on the CSAS. This may be particularly problematic for cases where the plasma is biased down, and therefore a significant fraction of power is found on the IBDV. An example of this type is shown in Fig. 5.1, based on the equilibrium information in Table 5.1.

Scan DivSOL 8-01	Common Scan Quantity	Value
g204118.00600_DivSol_8-01_1	I_p [MA]	2
g204118.00600_DivSol_8-01_6	B_T [T]	1
g204118.00600_DivSol_8-01_4	P_{inj} [MW]	10
g204118.00600_DivSol_8-01_5	betaN	4
g204118.00600_DivSol_8-01_2	---	---

Table 5.1: Scenario with ISP sweep on the IBDV that places some heat on CSAS.

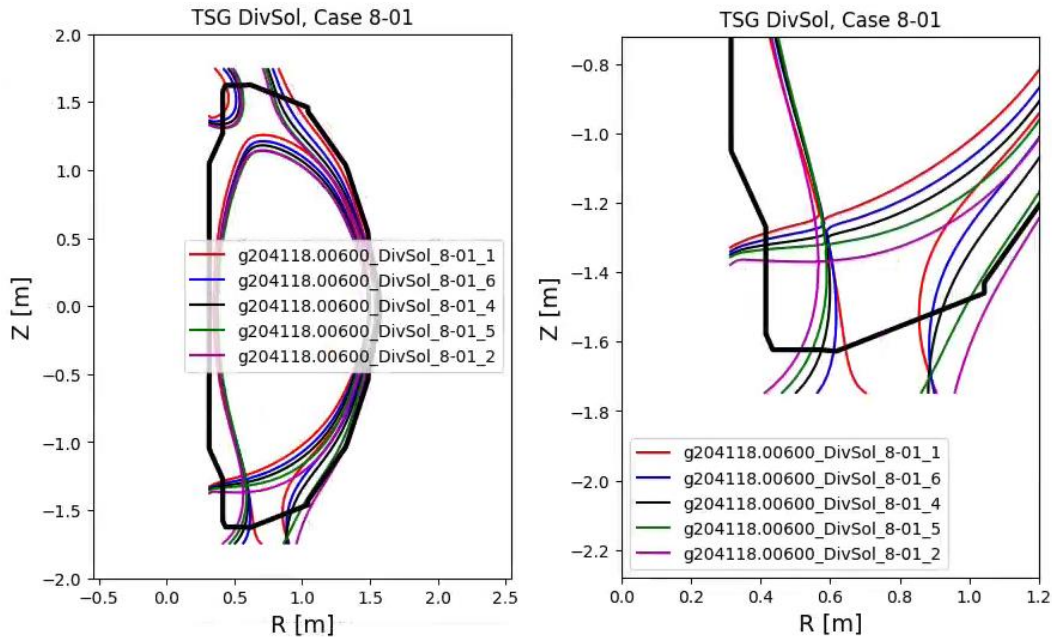


Fig. 5.1: Scan of plasma height in a $dr-sep = -1.5$ cm H-mode case.

The heat on the vertical section in this case is shown in Fig. 5.2. This case has an average swept power of 12 MW/m^2 on the vertical target. However, the IBDV section starts at $Z > -1.27$, and as can be seen in Fig. 5.1, the average swept power in this case is $< 2 \text{ MW/m}^2$. As shown in Fig. 5.2, field line angles are in the vicinity of 4-6 degrees on the portion of the CSAS illuminated with power

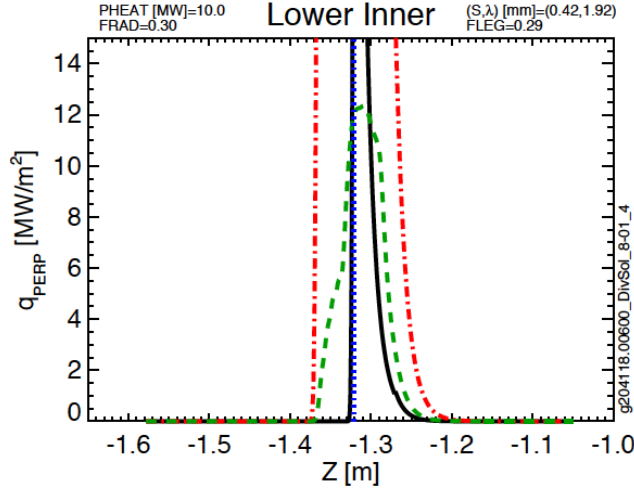


Fig. 5.2: Heat flux on the IBDV and CSAS from the case with sweeping of the ISP on the IBDV.

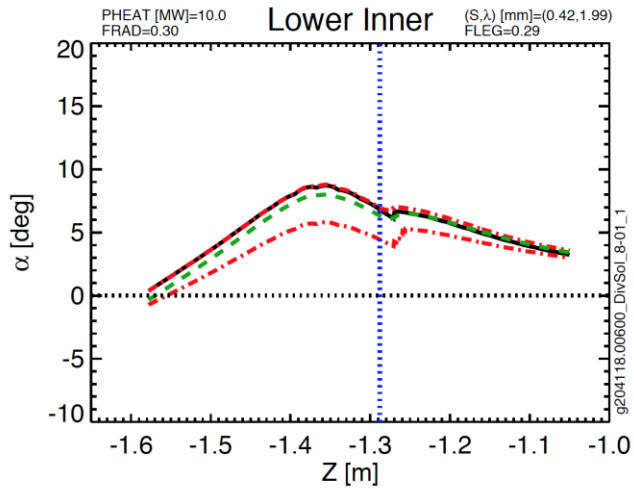


Fig. 5.3: Field line angles for case with sweeping of the ISP on the IBDV.

Scan	$[I_p, B_T, P_{heat}]$	dr_{sep}	Vertical Range of ISP Sweep	Peak Instantaneous Heat Flux	Peak Swept Heat Flux	Angle Range at Z_{min}	Angle Range at Z_{max}
---	[kA, T, MW]	cm	m	MW/m ²	MW/m ²	degrees	degrees
8-01	[2000, 1, 10]	-0.6	$ Z < 1.27$	15.0	3.0	5	7

Table 5.2: CSAS parameters for LSN H-mode case from DivSOL

Numerous other cases that place large heat fluxes on the high-heat-flux IBDV were studied, and are addressed in the memo on IBDV heat fluxes [1]. Those scans generally show a similar result, with time averaged powers of a ~ 3 MW/m² “spilling” over from the IBDV to the CSAS. There is a large uncertainty in these predictions since this depends on the inner divertor heat flux width scaling and the ability to control inner strike point position. Thus, while these cases should not drive PFC requirements, they represent a usage scenario for which the compatibility should be evaluated based on delivered CSAS

designs and results from initial commissioning. This could result in restrictions on the minimum $|Z|$ of the inner strike point.

6: H-Mode Scans on Row 4 Motivated by Materials and PFC TSG

The materials and PFC group conditions that put power in the large radius parts of the OBD for the purposes of putting power and particles in the vicinity of the MAPP probe [1]. The requirement for high fluence onto MAPP is the main driver and multiple discharges can be used to accomplish this, but ideally ~5 second pulses are desired. The heat flux and duration requirements can be adjusted if demanded by the OBD design engineers, but striving to reach what is listed in Table 6.2 and reflected in Table 2.3 represents a goal to efficiently execute MAPP experiments by minimizing the number of repeated discharges. Table 6.1 lists the equilibria and target plasma used to scope the Scenario 3 request from MPFC in [1]. Shape and heat flux results are shown in Figure 6.1-6.2 and listed in Table 6.2.

Scan	$[I_p, B_T, P_{heat}]$	dr_{sep}	Radial Range of OSP Sweep	Peak Instantaneous Heat Flux	Peak Swept Heat Flux	Angle Range at Z_{min}	Angle Range at Z_{max}
---	[kA, T, MW]	cm	m	MW/m ²	MW/m ²	degrees	degrees
3-02	[700, 0.7, 2]	-1.6	[0.90, 0.96]	9.1	3.0	9.0	9.7

Table 6.2: OBD parameters for LSN H-mode case from MPFC for MAPP testing

This result was used to develop the Case#4 requirement in Table 2.3 for the OBD-R4/5 region. The field line angle range was broadened as to accommodate a wider range of equilibria than the single case examined here.

Scan MPFC 3-02	Common Scan Quantity	Value
g116313.00860_MPFC_3-02_6	I_p [MA]	0.7
g116313.00860_MPFC_3-02_5	B_T [T]	0.75
g116313.00860_MPFC_3-02_1	P_{inj} [MW]	2
g116313.00860_MPFC_3-02_2	dr_{sep} [cm]	-1.6
g116313.00860_MPFC_3-02_3	---	---

Table 6.1: Scenario with OSP sweep on the OBD-R4.

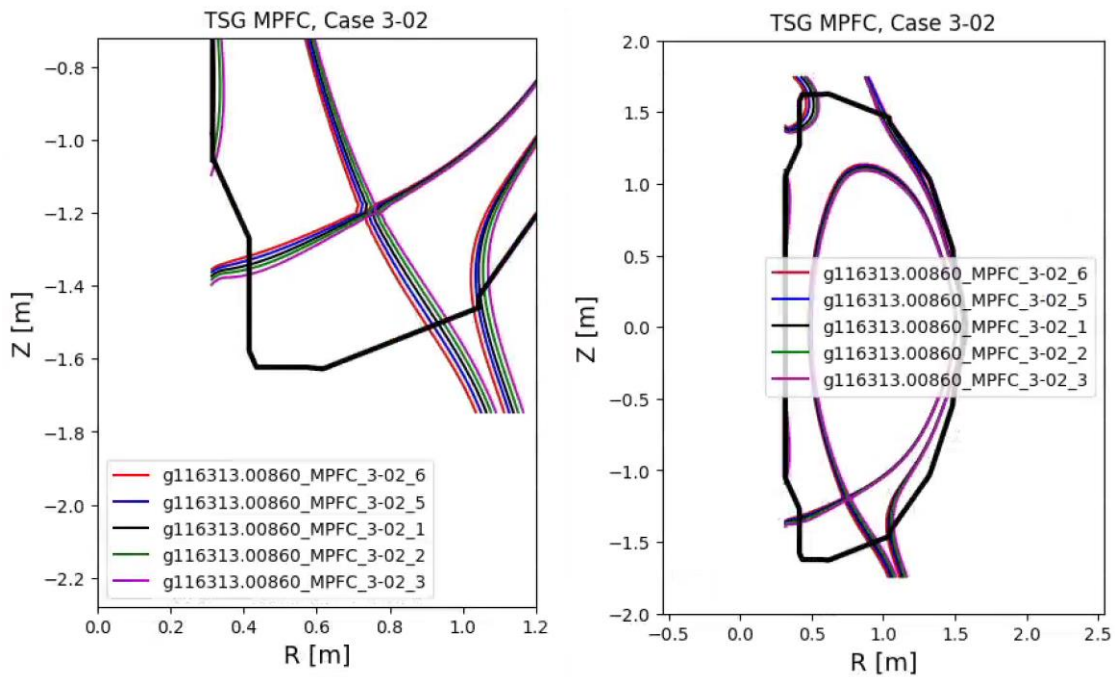


Figure 6.1: Equilibrium designed to put power in the vicinity of the MAPP probe.

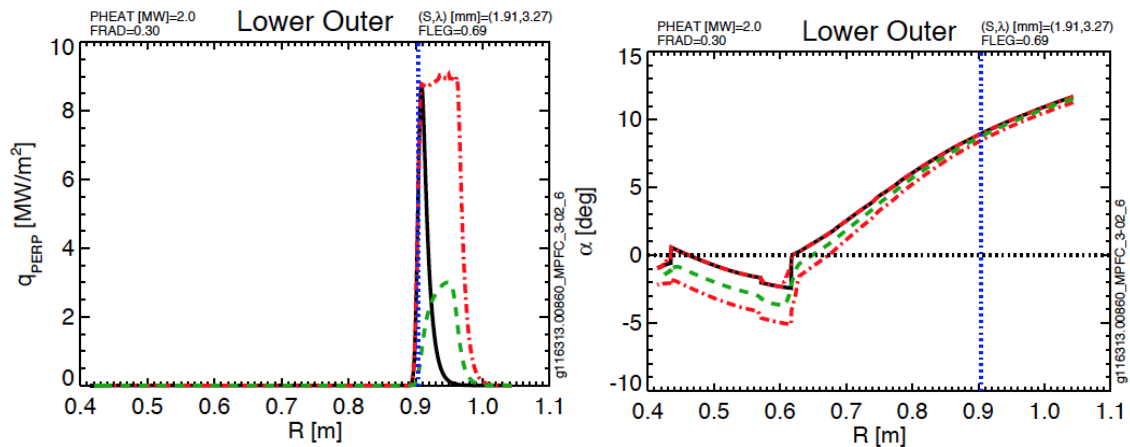


Figure 6.2: Heat fluxed for equilibrium designed to put power in the vicinity of the MAPP probe.

7: Lower Triangularity Scans That Place Power on Row 3 Tiles ($0.85 < R < 0.92$)

Multiple TSGs requested cases with low triangularity for physics studies. The elimination of using the IBDH for an inner strikepoint limits the creation of low triangularity plasmas to utilize the IBDV and the region around R3 on the OBD. An example is shown in Figures 7.1 and 7.2 for a case from the DivSOL TSG. These general span the high current, field and heating power but have physics goals that can be achieved on timescales of $\Delta t < 2.0$ seconds. These cases are summarized in Table 7.2, where it is evident that many far exceed any expected allowable. Some, such as PED 2-04, PED 2-16 and DivSOL 8-04 represent cases where the ISP was scanned, but the OSP scan was incomplete, indicating the difficulty of designing a combined IBDV and IBDH solution. These and other high heat flux scenarios will need to be revisited, using enhanced radiation power to bring heat fluxes to levels within the OBD R3 design limits. There are additional cases where the strike-point is located inboard of the $R=0.85$ tiles, but the heat flux extends onto OBD-R3. These are indicated in Table 7.3. Presently, a short-pulse, high power DivSOL and low power, long pulse MPFC request are used to define the heat flux and field line angle limits which should be used to drive design and are reflected in Table 2.2.

Scan	$[I_p, B_T, P_{heat}]$	dr_{sep}	Radial Range of OSP Sweep	Peak Instantaneous Heat Flux	Peak Swept Heat Flux	Angle Range at R_{min}	Angle Range at R_{max}
---	[kA, T, MW]	cm	m	MW/m ²	MW/m ²	degrees	degrees
PED, 2-04	[1400, 0.8, 8]	-1.5	[0.88, 0.89]	23.4	21.7	3.8	4.3
PED, 2-05	[1400, 1.0, 8]	-1.5	[0.81, 0.85]	29.1	15.4	2.7	5.2
PED, 2-16	[1800, 1.0, 10]	-1.5	[0.88, 0.89]	40.3	32.7	4.4	5.7
DivSol, 8-04	[1000, 1.0, 8]	-1.0	[0.84, 0.86]	15.3	12.4	2.3	3.3
DivSol, 8-05	[1800, 1.0, 10]	-1.0	[0.82, 0.88]	54.7	28.8	3.1	7.7
DivSol, 8-06	[1800, 1.0, 10]	-1.0	[0.80, 0.89]	55.7	12.4	1.4	7.9
DivSol, 8-07	[1000, 1, 7]	-1	[0.85, 0.9]	29.8	10.5	2.2	7.0
MPFC, 3-02	[700, 0.7, 2]	-1.6	[0.90, 0.96]	9.1	3.0	9.0	9.7

Table 7.2: OBD parameters for LSN+DN H-mode case from various TSGs. The range of the OBD R3 tiles in $0.85 < R < 0.92$

Scan DivSol 8-07	Common Scan Quantity	Value
g116313.008600_DivSol_8-07_6	I_p [MA]	1
g116313.008600_DivSol_8-07_5	B_T [T]	1
g116313.008600_DivSol_8-07_4	P_{ini} [MW]	7
g116313.008600_DivSol_8-07_1	betaN	4
g116313.008600_DivSol_8-07_2	dr_{sep} [cm]	-1
	Typical Lower Triangularity	

Table 7.1: Example parameters for a scan that places power on the Row 3 tiles ($0.85 < R < 0.92$)

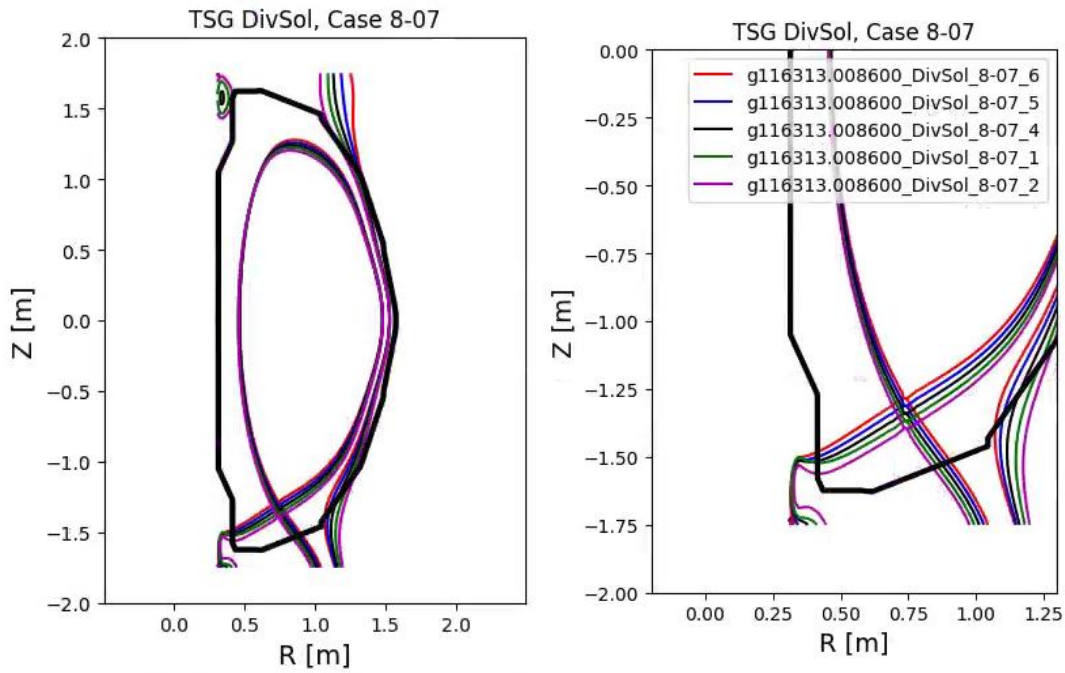


Fig. 7.1: A representative scan that places power on the Row 3 tiles.

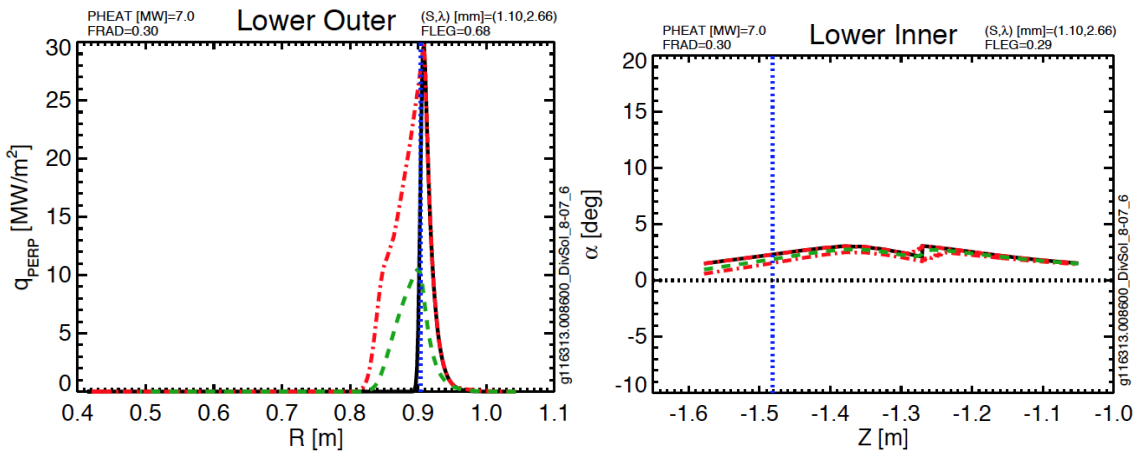


Fig 7.2: Lower outer target parameters for PED 2-05, a scan that places power on the Row 3 tiles

Scan	[I_p, B_T, P_{heat}]	dr_{sep}	Radial Range of OSP Sweep	Peak Instantaneous Heat Flux	Peak Swept Heat Flux	Angle Range at $R=0.85$
---	[kA, T, MW]	cm	m	MW/m ²	MW/m ²	degrees
PED, 1-05	[1200, 0.65, 6]	-1.5	[0.80, 0.84]	15	9	5
PED, 1-17	[1200, 0.65, 10]	-1.6	[0.80, 0.84]	25	14	5
PED, 2-05	[1400, 1.0, 8]	-1.5	[0.81, 0.85]	30	16	4
DivSol, 8-03	[1000, 1.0, 8]	-1.0	[0.73, 0.84]	19	4	4

Table 7.3: OBD parameters for LSN+DN H-mode cases that put the strikepoint inboard of Row 3, but may have some power spill over. The range of the OBR R3 tiles at $R=0.85$ which decays strongly for $R > 0.85$.

Examples in Table 7.3 place large heat fluxes on the lower major radius portion of OBD-R3, and have values that are above that expected for this region to support. These may be compatible with further heat flux mitigation such as increased radiation. There is a large uncertainty in these predictions since this depends on the outer divertor heat flux width scaling and the ability to control outer strike point position. Thus, while these cases should not drive PFC requirements, they represent a usage scenario for which the compatibility should be evaluated based on delivered OBD-R3 designs and results from initial commissioning.

References

- [1] Memo PFCR-MEMO-009-00: *Heat Fluxes on the Vertical Target*
- [2] Memo: PFCR-MEMO-010-00: *Heat Fluxes on the IBDH and OBD Row 1 and Row 2*
- [3] Memo DivSol-170524-VS-02: *Impact of Polar Regions on DivSol Research*
- [4] Memo ASC-170523-DB-02, *Impact of Proposed Polar Region Modifications on Research and Scenarios for ASC Topical Science Group*
- [5] Memo PED-171805-AD-02: *Impact of Potential Polar Region Modifications on Research and Scenarios for TSG-PED.*
- [6] Memo TT-170523-WG-01, *Impact of Potential Polar Region Modifications on Research and Scenarios for Transport and Turbulence Topical Science Group*
- [7] Memo MS-170523-JN-04: *Impact of Potential Polar Region Modifications on Research and Scenarios for the Macroscopic Stability Topical Science Group*
- [8] Memo MPFC-170523-MJ-02: *Impact of Potential Polar Region Modifications on Research and Scenarios for the Material and Plasma Facing Components Topical Science Group*

Record of Changes

Rev.	Date	Description of Changes
0	7/25/17	Initial draft release to PFCR-WG and to Recovery
1	9/11/17	Changed 'TO' from Hawryluk to Menard to reflect leadership change and added Record of Changes Section

Suggested Distribution

Doug Loesser
Mike Mardenfeld
Brian Linn
Ankita Jariwala
Nate Dean
Andre Khodak
Marc Sibiliala
Dang Cai
Peter Titus
Art Brooks
Bob Ellis
Filippo Scotti
Vlad Soukhanovskii
Mike Jaworski
Devon Battaglia
Ahmed Diallo
Jack Berkery
Walter Guttenfelder
Stan Kaye
Rajesh Maingi
NSTX-U File